Modeling of a MEMS Floating Element Shear Sensor

Nikolas Kastor [1], Zhengxin Zhao[1] and Robert D. White[1]
[1] Mechanical Engineering Department, Tufts University, Medford, MA, United States.

ABSTRACT

A MEMS floating element shear stress sensor has been developed for flow testing applications, targeted primarily in ground and flight testing of aerospace vehicle and components. However, concerns remain about the interaction of the flow with the mechanical elements of the structure at the micro-scale. In particular, there are concerns about the validity of laminar flow cell calibration to measurement in turbulent flows, and the extent to which pressure gradients may introduce errors into the shear stress measurement. In order to address these concerns, a numerical model of the sensor has been constructed.

In this paper, a computational fluid dynamics (CFD) model is described. The CFD model directly models a laminar flow cell experiment that is used to calibrate the shear sensor. The computational model allows us to quantify the contributions (e.g. pressure gradient vs. shear, top surface vs. lateral surfaces) to the sensor output in a manner that is difficult by purely experimental means. The results are compared to experimental data, validating the model and resulting in the following: Surface shear stress contributes approximately 40% of the total flow direction force; pressure gradient effects contribute nearly 45% for the textured shuttle described here; lift forces and pitching moments are non-zero. Thus, it is found that flow interactions are complex and that it is insufficient to simply assume that flow forces on the sensor are the top area multiplied by wall shear, as is sometimes done. Pressure gradient effects, at least, must be included for accurate calibration.

INTRODUCTION

Wall shear stress and skin friction are important measurement values in flow testing of vehicles and devices in aerospace applications. Existing techniques, such as oil film interferometry, boundary layer profile surveys, or thermal methods, can be used to determine these values, but the measurements can be difficult to apply, are indirect and may not provide real time data [1, 2]. Direct floating element MEMS sensors address these issues by providing real-time, momentum transfer based, unsteady shear measurements at a surface, with the potential for low topology, and array sensing in multiple directions. The shear sensor modeled here, shown in Figure 1, has been described previously by our group [3, 4]. The device is fabricated using surface micromachining on a glass substrate. The structure itself is 8 micron thick electroplated nickel, with 12 micron tall raised posts on the top surface. The structure is separated from the glass substrate by a 5 micron high air gap. The comb fingers are 5.2 microns wide with 2.8 micron air gaps. Additional details regarding geometry and fabrication can be found in the reference [3, 4].

As flow passes over the device, hydrodynamic forces cause the sensor to deflect, creating a differential capacitance change in the two sets of comb fingers. Ideally, the differential capacitance change would be linearly related to surface shear, and insensitive to other forces. However, this will not always be the case. A numerical model was created in order to quantify the various hydrodynamic forces, and, in particular, to understand how stream-wise pressure

gradients can act as an error source in the measurement of surface shear. The model is broken into three parts: Determination of forces applied by the flowing fluid; the deflection of the sensing element as a result of those fluid forces; and the correlation of that deflection with a change in capacitance. This paper will focus on the fluid model.
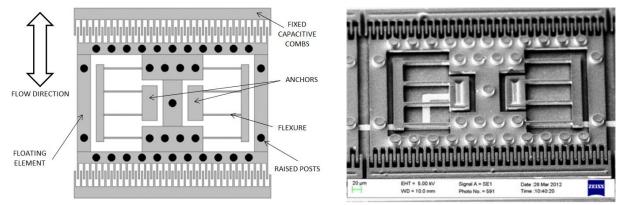

Figure 1. The floating element shear stress sensor produced in the MEMS laboratory of Tufts University.

THEORY

It is often assumed that the stresses acting on a floating element sensor are only proportional to the local velocity profile and viscosity of the fluid. While this assumption is correct for the stress acting on a flat surface, the shear sensor is a 3D body that interacts in a more complex fashion with the flow. The output signal of the shear sensor is therefore expected to depend on pressure gradient as well as local shear, and potentially, on other features of the flow. A conceptual forcing model that incorporates both shear and pressure gradient forcing is shown in Figure 2 below.
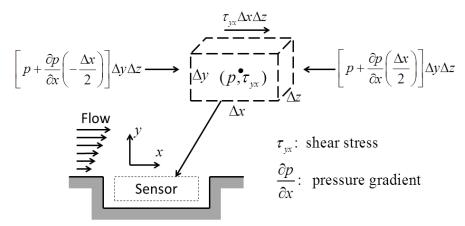

Figure 2. Fluid-sensor interaction including shear and pressure gradient.

The force on the stress sensor can then be estimated by equation (1),

$$F = \tau_{yx} \cdot \Delta x \Delta y - \left(\frac{\partial P}{\partial x}\right) \cdot \Delta x \cdot (\Delta y \Delta z) \tag{1}$$

where Δx, Δy and Δz are the effective element size, τ_{yx} is the shear stress in the flow direction and $\partial P/\partial x$ is the pressure gradient along the flow direction. Expanding on this notion, a three-dimensional model of the sensor was created where the total force and moment are extracted from surface integrals of the relevant pressures and shear stresses over the entire periphery of the sensor,

$$\Sigma F_x = \int_A \left[\sigma_{xx} + \tau_{zx} + \tau_{yx} \right] dA - xk_x - xC_x = 0 \tag{2}$$

$$\Sigma F_y = \int_A \left[\sigma_{yy} + \tau_{zy} + \tau_{xy} \right] dA - yk_y - yC_y = 0 \tag{3}$$

$$\Sigma F_z = \int_A \left[\sigma_{zz} + \tau_{xz} + \tau_{yz} \right] dA - zk_z - zC_{cz} = 0 \tag{4}$$

$$\Sigma M_\theta = \int_A \left[y\sigma_{zz} + z\tau_{zy} + z\sigma_{yy} + y\tau_{yz} + y\tau_{xz} + z\tau_{xy} \right] dA - \theta k_\theta - \theta C_\theta = 0 \tag{5}$$

$$\Sigma M_\phi = \int_A \left[x\sigma_{zz} + z\tau_{zx} + x\tau_{yz} + z\tau_{yx} + z\sigma_{xx} + x\tau_{xz} \right] dA - \phi k_\phi - \phi C_\phi = 0 \tag{6}$$

$$\Sigma M_\psi = \int_A \left[x\tau_{zy} + y\tau_{zx} + x\sigma_{yy} + y\tau_{yx} + y\sigma_{xx} + x\tau_{xy} \right] dA - \psi k_\psi - \psi C_\psi = 0 \tag{7}$$

Subtracted from this hydrodynamic force is the mechanical spring force due to sensor displacement. Also subtracted from the total stress is a model of the electrostatic restoring force created by the capacitive combs. This force is represented by a coefficient C that acts as an equivalent electrostatic spring. In this paper we will focus on the hydrodynamic forces.

COMPUTATIONAL FLUID DYNAMICS ANALYSIS

Forces acting on the sensor by the flowing fluid were determined numerically by a computational fluid dynamics study. The shear sensor model was cut in half along the center line, to take advantage of symmetry, and subtracted from a control volume. The height of the control volume is the height of the flow-cell where the physical sensor was tested [3]. The inlet boundary condition was defined as a parabolic velocity profile for fully-developed, laminar flow in a rectangular duct and a zero-pressure boundary condition was chosen for the outlet, also in imitation of actual test conditions. Because the inlet velocities being tested in this model are below Mach 0.3, an incompressible air model was used with a density of 1.21 kg/m^3 and a dynamic viscosity of 2×10^{-5} Pa·s. In imitation of test conditions, the inlet flow rates were chosen from 5 CFH to 40 CFH, in 5 CFH increments. At these flow rates, the flow will remain laminar. Channel height was also varied in imitation of test conditions from 200 μm to 500 μm. Independent variation of channel height and flow rate results in a variety of pressure gradient and surface shear conditions.

Limited by the CFD software, the geometry was meshed with 2nd-order tetrahedral elements instead of a more advanced element. To minimize error, the mesh was refined with 10 elements across narrow flow regions. This model was solved with a stationary, nonlinear, iterative, GMRES solver to produce a stable and fully converged solution.
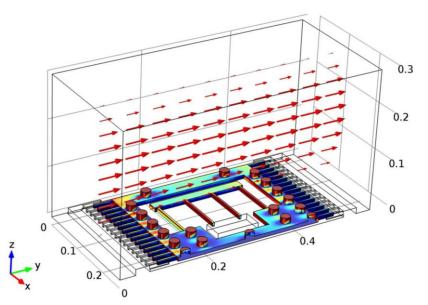
Figure 3. A typical CFD solution showing the velocity profile (arrow plot) and total stress (surface plot).

Integrating the shear stress over the surfaces of the floating element yields the applied force. These results were collected for different configurations of channel height and inlet flow rate. Below, force curves are plotted as a function of Reynolds number based on average inlet velocity and channel hydraulic diameter. In addition, as shown in the figure, force depends on relative roughness, which is defined as the ratio of sensor height (25μm) to channel height. It is emphasized that the CFD model was conducted with the full, three-dimensional, post geometry, as shown in Figure 3. However, when presenting the results from the model, it is found that force depends on at least two length scales: the height of the duct and the height of the element. Two non-dimensional numbers are needed to parameterize the results and, in imitation of Moody charts, Reynold's Number based on hydraulic diameter of the flow slot is used as the primary non-dimensional quantity. A "relative roughness", defined as the structure thickness (25 μm) divided by channel height (which varies over the computational cases from 0.2 to 0.5 mm), is used as the second non-dimensional parameter. It is found that by using these two non-dimensional parameters, all computational cases collapse onto smooth curves, as shown in Figure 4. The Y-direction force is the stream-wise force, that is, the total drag on the structure. The Z-direction force is the out-of-plane force, that is, the total lift on the structure. The moment about the X-axis is a pitching moment. Due to symmetry, there is no net force in the cross-flow direction, nor is there net moment about Y (roll) or Z (yaw).

The forces on the sensing element are broken down into three major contributors: (i) viscous stress on the main element, (ii) net pressure effects (i.e. related to pressure gradient) on the main element and (iii) the total stress on the raised cylindrical posts. As seen in Figure 5, in the flow direction (y direction), the pressure gradient contributes from 20% to 25% of the total stress. The viscous stresses on the main element itself contribute only about 40% of the total force at low Reynolds numbers. This drops to 30% as the Reynolds number increases. The relative decrease in viscous stress is, of course, accompanied by a relative increase in the contribution of the raised posts and pressure gradient. An important consequence of this is that laminar flow cell calibrations must independently account for pressure gradient and viscous effects. If pressure gradient effects are ignored, and the entire force is ascribed to viscous forces, the calibration will substantially overestimate sensitivity, on the order of 50-70%.
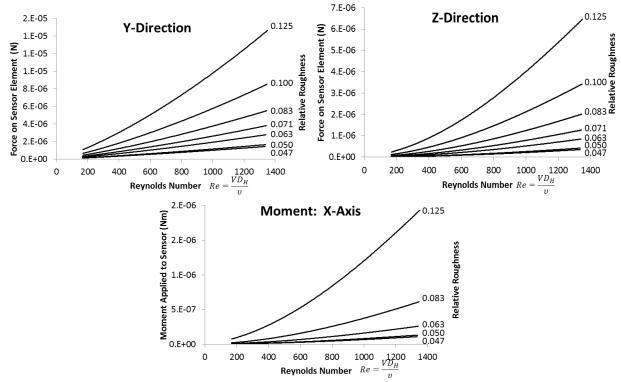
Figure 4. CFD data showing the traction on the floating element as a function of Reynolds number and relative roughness.

As seen in Figure 5, the force in the flow direction on the posts accounts for 40-45% of the total force on the structure. Thus, adding the posts significantly increases device output in flow. However, it is not readily apparent that this force is primarily a shear stress contribution. Indeed, it seems likely that the post stresses are driven mainly by stream-wise pressure gradients, although additional work needs to be done to fully understand the effect.
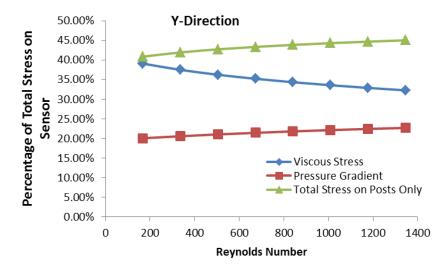

Figure 5. Plot showing the relative contribution of pressure gradient, viscous shear stress, and total stress on the raised posts to the total force on the sensing element for different Reynolds numbers at an intermediate relative roughness of 0.083.

COMPARISON TO MEASUREMENTS

The sensor has been calibrated in a laminar flow cell with identical geometry to the CFD modeling performed in this paper, as shown in Figure 6, where the details of the measurement methods are described in our previous work [3,4]. Essentially, the system consists of a wide but shallow slot through which compressed air is driven and controlled by an electronic mass flow controller. The flow rate is independently verified using a sequence of static pressure taps along the flow, which measure the pressure gradient. The sensor is far enough down the flow cell that a fully developed Poiseuille profile is established. Flow rates are kept low enough that the flow remains laminar. By varying the slot height and the flow rate, the stream-wise pressure gradient and wall shear can be independently varied, as described in [4].
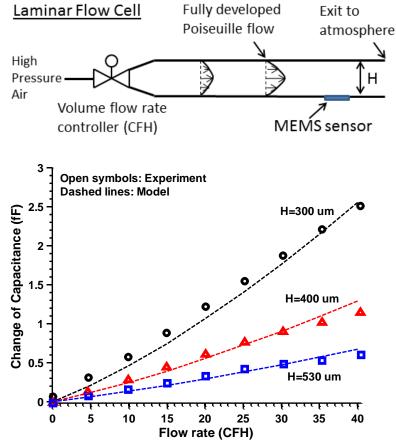

Figure 6. (Top) a laminar flow cell was used to deliver Poisseuille flow at various flow rates and channel heights to the sensor. (Bottom) Comparison of measured (open symbols) and modeled (dashed lines) capacitance change at 3 channel heights and 9 flow rates.

In order to relate the force, as predicted by the CFD calculation in Figure 4, to the measured capacitance change, as detected by the electronics in Figure 6, a structural and electrostatic model are needed. Three dimensional numerical models have been constructed but are not described here due to paper length restrictions. However, a simple analytical model of the structural mechanics and electrostatics, which simplifies some of the three dimensional effects, has been described in [4] by:

$$\Delta C = M \frac{N \varepsilon L^3}{Edw^3} \sum F_y \qquad (8)$$

where *M=128* is the number of elements in the array that act in parallel, *N=64* is the number of fingers attached to each floating element, ε is the permittivity of free space, *L=99 μm* is the length of the beam flexure, *E=205 GPa* is the modulus of the structural nickel, *d=2.8 μm* is the gap between comb fingers, and *w=5.1 μm* is the width of the beam flexures. In this model, the sensor responds only to forces in the flow direction (F_y), and the output is a change in capacitance (ΔC). Figure 6 shows a comparison between the measured differential capacitance change (open symbols) and the predicted capacitance change (dash lines) for 3 different duct heights and 9 different flow rates.

The measured changes in capacitance are a very good match to the change predicted by the CFD model coupled to the simple analytical structural and electrostatic model. No fitting parameters were used; all geometric parameters were taken from scanning electron microscope images of the sensor, and the single material property, the modulus of Nickel, is an accepted bulk value. This match strongly validates the CFD model. Small discrepancies observed between the measurement and model could be due to the lift forces or pitching moments discovered during the CFD modeling, which are not included in the above electrostatic/structural analysis.

CONCLUSION

A computational fluid dynamics simulation has been carried out to investigate the hydrodynamic performance of a MEMS floating element shear stress sensor and validate against measurement. The forces and moments acting on the sensor body were determined, where total force is a function of both Reynolds number and relative roughness under laminar flow conditions. Surface shear accounts for approximately 40% of the total hydrodynamic force on the element, with the remainder coming from pressure gradient effects and surface topography. Lift forces and pitching moments are non-zero. Future designs should endeavor to increase the shuttle top surface area, and reduce gaps and projected frontal area in order to minimize pressure gradient sensitivity and maximize shear sensitivity. In addition, more analysis should be conducted on the lift forces and pitching moments to determine their effect on the sensor output. Finally, it is recommended that a methodology similar to the one adopted in [4] be used to independently and experimentally determine shear and pressure gradient sensitivity. This is because pressure gradient sensitivity can be significant for floating element shear sensor designs, particularly in laminar slot flow environments commonly used for calibration where stream-wise pressure gradients are typically high.

REFERENCES

1. H. H. Fernholz, G. Janke, M. Schober, P. M. Wagner and D. Warnack, "New developments and applications of skin-friction measuring techniques,"Measurement Science and Technology, vol. 7, pp. 1396-1409, 1996.
2. J. W. Naughton and M. Sheplak, "Modern developments in shear-stress measurement,"Prog.Aerospace Sci., vol. 38, pp. 515-570, 0, 2002.
3. Z. Zhao, M. Shin and R. D. White, "A MEMS floating element with bump shear stress sensor array on a chip," 51st AIAA Aerospace Sciences Meeting Including the New

Horizons Forum and Aerospace Exposition, Grapevine (Dallas/Ft. Worth Region), Texas, 2013.

4. Z. Zhao, M. Shin, J. M. Gallman and R. D. White. "A Microfabricated Shear Sensor Array on a Chip with Pressure Gradient Calibration", *Sensors and Actuators A: Physical*, vol. 205, pp. 133-142, 2014.